

Tunable band-pass plasmonic waveguide-filter in the near infrared region

G KhosroBeygi¹, M R Jafari² and M Shahmansouri^{1,3*} 

¹Department of Physics, Faculty of Science, Arak University, Arak, Iran

²Department of Condensed Matter Physics, Faculty of Physics, Alzahra University, Tehran, Iran

³Department of Atomic and Molecular Physics, Faculty of Physics, Alzahra University, Tehran, Iran

Received: 03 November 2023 / Accepted: 29 July 2024

Abstract: A tunable multi-channel band-pass plasmonic filter in the near-infrared range is investigated using the finite element numerical method (FEM). The structure of the proposed waveguide filter consists of several dielectric slots sandwiched between two metal layers. The slots are filled with air and silica. Numerical analysis and simulation demonstrate that the number of bandpass channels, amplitude, intensity, and bandwidth can be adjusted by changing the geometrical parameters such as material, length of each slot, width, and number of intermediate slots in the filter. The proposed filter was studied in the wavelength range of 1–4 μm , exhibiting 2 to 5 transmission peaks with varying transmission powers. Given that the incident wavelength in this article is larger than the dimensions of the waveguide and slot, this structure can focus the light within a sub-wavelength scale. The proposed structure is expected to be used as an essential component of photonics devices due to its ability to confine light in the sub-wavelength region, simple fabrication, and multi-channel operation.

Keywords: Band-pass; Plasmonic waveguide-filter; Near-infrared

1. Introduction

Plasmonic waveguides and filters constitute an intriguing research field that has captured the attention of numerous researchers in recent years [1–7]. Surface plasmon-polariton waves (SPPs) arise from electronic excitations at the metal–dielectric interface, resulting to confined electromagnetic structures. Due to the potential for simultaneous transmission of optical and electronic waves within such structures, plasmonic waveguide filters have opened up new research fields and applications [8–10]. The coupling between the incident wave and a plural oscillation of electrons at the metal–dielectric interface excites surface plasmon polaritons (SPPs) [11, 12]. One of the important features of surface plasmons that has attracted the attention of researchers is the ability to focus on a region smaller than the wavelength. This feature could provide a way to overcome the common limitations of traditional optics [13]. Controlling light at dimensions below the wavelength

remains a challenging issue in nano-photonics [1]. Surface plasmon-polaritons provide a means to achieve this control, leading to intriguing outcomes in various fields, including optical switches [14, 15], filters [1–7], sensors [16], optical splitters [17], absorbers [18], waveguides [1–7, 13, 19–25], Raman spectroscopy [26], sensors [27], and couplers [28]. SPP-based filters have garnered attention due to their compact dimensions, low relative angular error, tunability for pass or stop spectra, and suitability for both wide and narrow bands [12]. Despite significant efforts in developing plasmonic filters [29–33], researchers continue to explore ways to enhance their performance.

Recently, based on the studies conducted on the traditional plasmonic materials (gold and silver), metal-insulator-metal (MIM) filters with these materials have been proposed and investigated [34]. Some investigations have focused on the band-pass plasmonic filters based on a slot cavity [35, 36] and the effect of the slot cavity on the transmission spectrum. Researchers demonstrated that by selecting proper input and output waveguide positions, the resonance characteristics of the slot cavity and the out-coupling strength can be effectively modified. Another

*Corresponding author, E-mail: mshmansouri@gmail.com

surface plasmon polaritons (SPPs) narrow band-pass filter based on a slot cavity has been proposed by Hu and Zhou [37]. By varying the positions of output waveguides, the filter exhibited the spectrally splitting function [37]. In Pav's research, a diaphragm coupling mechanism and slot method with an added stub in the cavity have been employed [38]. Pav aimed to achieve an almost complex structure to increase the number of output channels. All the mentioned works above operate in the wavelength range of 0.6–1.8 μm . Although these methods achieved relative success in their works, one of the important factors is the ease of constructing the filter, which was not easily achievable. This motivated us to investigate a filter structure with a straightforward design while also being multi-channel.

In this paper, to obtain a multi-channel and narrow-pass spectrum in the wavelength range of 1–4 μm (75–300 THz), a novel structure of MIM filter was proposed. The filter design involves slots aligned in the direction of wave propagation, which are sandwiched between the metal layers. According to Fig. 1, silver is used as metal; air and silicon are used as dielectrics. The MIM plasmon filter, in the range of 1–4 μm (75–300 THz), is proposed, which can be utilized in applications such as infrared spectroscopy, medical diagnostics, and astronomical imaging [39]. The filters that work in the infrared frequency range usually have large dimensions. In contrast, the structure of the proposed filter includes several dielectric slots with different materials that are created inside the metal. In the following sections, two different structures for plasmonic waveguide filters are proposed and described.

2. Filter structure and formulation

A schematic view of the proposed filter is shown in Fig. 1, consisting of two air slots as the inlet and outlet of the filter and a middle silica slot surrounded by two layers of silver. Materials in the gray, yellow, and green areas are corresponded to silver, air ($\epsilon_{air} = 1$), and silica ($\epsilon_{SiO_2} = 1.45$), respectively. Parameters for the filter structure are presented in Table 1.

Since the width of MIM waveguides is much smaller than the incident wavelength, only the main TM mode is excited in the structure, and its dispersion relation is expressed by the following equation [37]:

$$\epsilon_d k_m + \epsilon_m k_d \tan h\left(\frac{k_d}{2}\omega\right) = 0 \quad (1)$$

where k_d and k_m are given by $k_d = (\beta^2 - \epsilon_d k_0^2)^{1/2}$ and $k_m = (\beta^2 - \epsilon_m k_0^2)^{1/2}$. Also ϵ_d and ϵ_m are, respectively, the dielectric constants of insulator and metal layers. Since silver metal is used in the present structure, its permittivity is govern by the following equation based on the Drude model [1, 26]:

$$\epsilon_m(\omega) = \epsilon_\infty - \frac{\omega_p^2}{\omega(\omega + i\gamma)} \quad (2)$$

where the background dielectric constant is $\epsilon_\infty = 3.7$, the damping frequency of the oscillations is represented by $\gamma = 2.634 \times 10^{16} \text{ Hz}$, $\omega_p = 1.38 \times 10^{16} \text{ Hz}$ [1, 27] denotes the bulk plasma frequency, and ω shows the angular frequency of the incident light.

When the light beam enters the filter from the input port, only the TM mode can be excited and propagated within

Fig. 1 Schematic diagram of the proposed plasmonic slot filter

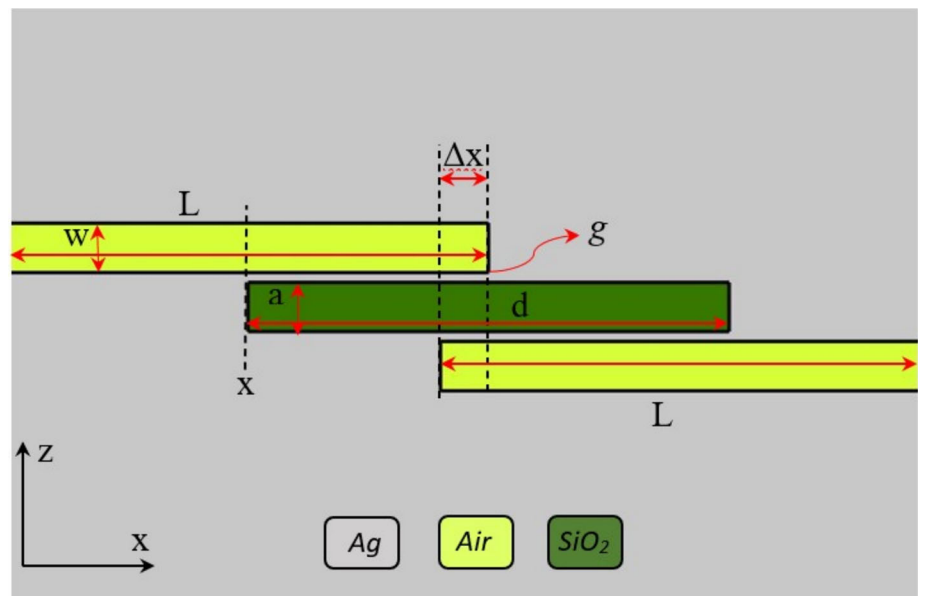


Table 1 Structure parameters of the proposed plasmonic filter

Parameters	Values(nm)
Width of Air slot (W)	50
Width of SiO ₂ slot (a)	30 < a < 150
The length of the air slot (L)	300 < L < 600
The gap between two slots (g)	10
The length of the SiO ₂ slot (d)	200 < d < 690
Overlapping of two air slots (Δx)	50
Location of the edge of the SiO ₂ slot (x)	L/2
Total length of the filter	850 ~ 1150
Total width of the filter	1000

the filter channel. A portion of the excited SPPs passes through the filter channel. Subsequently, interference occurs between the reflected SPPs and the transmitted portion. A phase difference between the reflected and transmitted SPPs is given by $\theta = \varphi + 2k_s L$, with k_s being the SPPs wavevector, and φ denotes the phase shift due to the reflections at the end of the teeth. When φ becomes even (odd) multiple of π , the transmission is maximum (minimum). The response wavelength of an excited SPPs follows the following form:

$$\lambda_t = \frac{4n_{eff}L}{(2m+1)\pi - \varphi} \quad (3)$$

where λ_t denotes the transmission wavelength, L is the length of the slot cavity, φ represents the phase shift due to the reflection at the dielectric-metal interface, and m is an integer number. An effective refractive index of the slit waveguide, n_{eff} , depends on the waveguide's medium and width [3, 40]:

$$n_{eff}^2 = \varepsilon_d^2 + \frac{\lambda \varepsilon_d^2}{\pi w} \left(\frac{\varepsilon_d - \varepsilon_m}{\varepsilon_m} \right) \quad (4)$$

where w denotes the width of the dielectric, λ is the incident wavelength, and ε_m and ε_d are the relative dielectric constants of the metal and dielectric layers, respectively.

3. Results and discussion

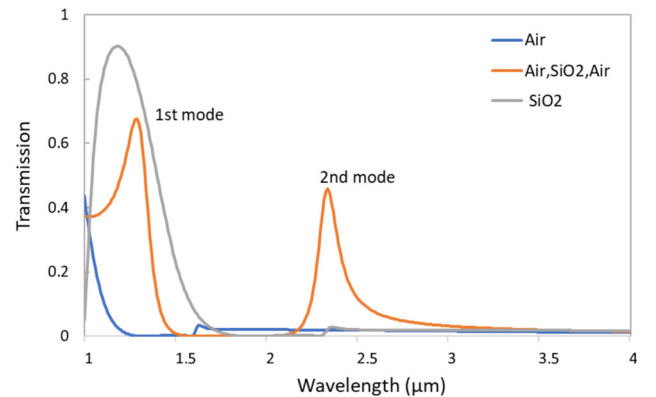
The geometric structure of the proposed filter combines of three rectangular dielectric slots made of the different materials. Specifically, between the two layers of silver (Ag), there are two rectangular slots of air serving as inlet and outlet ports, along with a rectangular slot of silica (SiO₂). The structural parameters of the filter are presented in Table 1. The work started with the physical study of the filter performance (length slot, number of slots, gap width, and geometry) within a target wavelength band (THz) to

achieve both high transmission efficiency and a narrow bandwidth. The silver is chosen for its ability to excite the SPPs, while SiO₂ fills the intermediate slot and tunes the wavelength band gap to the THz range. The FEM employing COMSOL Multiphysics version 5.6 is used to model the proposed filter's performance.

3.1. Effect of materials slots on the transmission spectrum

In the first step, the material of the slots is changed (as shown in Fig. 1) and the transmission spectrum is obtained from the simulation results. Initially, all three slots are filled with air. In the subsequent step, they are filled with silica. Finally, the inlet and outlet slots are filled with air, while the middle slot contains silica material. Figure 2 illustrates the filter transmission spectrum for the above cases.

The air slot has a width of $w = 50$ nm and the silica slot has a width $a = 50$ nm. A length of the air slots is $L = 500$ nm, and the silica slot length is $d = 500$ nm. A gap between the two slots is $g = 10$ nm. The wavelength range studied is from 1 to 4 μm , the wavelength increases by 0.01 μm in each step to reach from 1 to 4 μm Figure 2 reveals that when all slots are filled with air, nearly the entire incident wavelength range is blocked, allowing only a small portion at the beginning of the range to pass through. When all slots are filled with silica, a strong resonance mode appears at $\lambda = 1.18$ μm with a transmission power of 0.90, although its bandwidth is wide. When the two side slots contain air and the middle slot is filled with SiO₂, two narrow resonance modes appear at central wavelengths of $\lambda = 1.29$ μm and $\lambda = 2.34$ μm , respectively, with the transmission power of 0.67 and 0.46. At this stage, only the type of dielectric material and its arrangement have changed. Consequently, the effective refractive index changes, resulting in a change in the

**Fig. 2** Transmission spectra for different slot materials

transmitted central wavelength. These results correspond to Eqs. (3) and (4).

3.2. Effect of air slot length on the transmission spectrum

In the second example, based on the last previous state that had two resonance modes, the two inlet and outlet slots were filled with air, and the middle slot is filled with silica. Then, the effect of the length of the air slots is investigated. Therefore, the length of the air slits is changed from $L = 300$ nm to $L = 600$ nm and the transmission spectrum is plotted. The values of other parameters are similar to the previous example, except for the length of the silica slot, which was set to $L = 400$ nm. Figure 3 represents the transmission spectra of the depicted filter for different air slot lengths with $w = 50$ nm. It has been observed that the length of the air slot does not significantly affect the transmission power and the wavelength of the transmission. In all cases, when the incident wavelengths are $\lambda = 1.08$ μm and $\lambda = 1.90$ μm , the filter allows them to pass, while the rest of the incident wavelengths are blocked within the studied domain. The two wavelengths corresponding to the 1st and 2nd resonance modes are $\lambda = 1.08$ μm and $\lambda = 1.90$ μm , respectively, with transmission powers of 0.82 and 0.53.

3.3. Effect of the length of the intermediate slot (SiO_2) on the transmission spectrum

In the third example, the slot length of the SiO_2 was changed from $d = 200$ nm to $d = 690$ nm, and again, the incident wavelengths started from 1 μm and continued with an increase of 0.01 μm in each step until it reached 4 μm . The transmission spectrum was plotted. The other parameter values are $a = w = \Delta x = 50$ nm, $L = 500$ nm, $x = L/2$, and $g = 10$ nm. A simulation result and transmission spectrum are shown in Fig. 4. At each length, two resonance modes occurred. The first mode is located in the initial region of the wavelength range, and

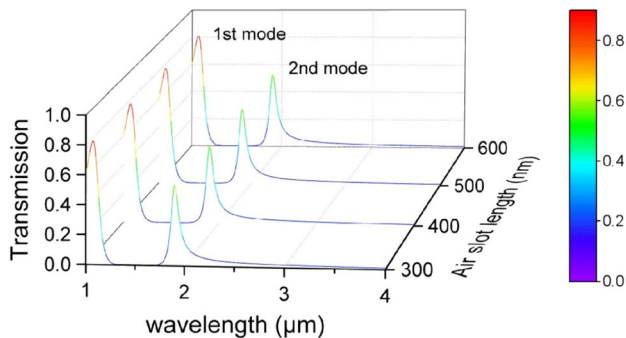


Fig. 3 The transmission spectra for different air slot lengths (L)

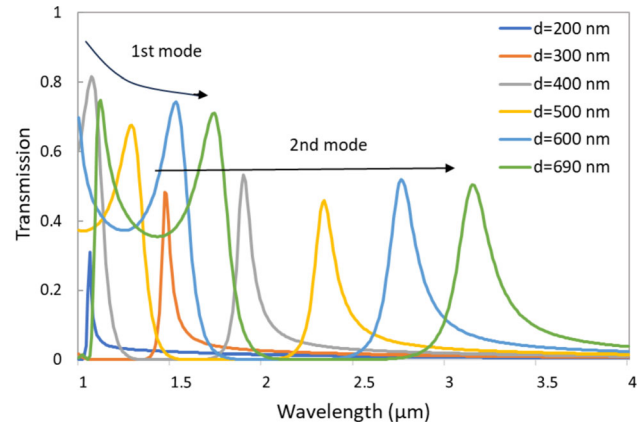


Fig. 4 The transmission spectrum for different lengths of SiO_2 slot (d)

the second mode is extended to the longer wavelengths. By increasing the slot length of the SiO_2 , the transmitted wavelengths are shifted to longer values. This shift is more significant for the second mode. The length of 400 nm exhibits more suitable power and width for the slot than the other lengths, which may be due to the appropriate phase change in this slot length compared to the other slot lengths.

Figure 5 illustrates the relationship between the resonance mode shift and the magnitude of the slot length. As shown in Fig. 5a, increasing the length of the SiO_2 slot results in a redshift of the resonance modes, corresponding to Eq. (3). The transmission to the longer wavelengths is more pronounced in the second mode. Simultaneously, the transmission peaks of the first mode exhibit less redshift, indicating that the shorter wavelengths are less dependent on the slot length. In the other words, the blue graph (representing the 1st mode) shows a linear shift in the resonance wavelength that has a gentle slope, while the orange graph (representing the 2nd mode) exhibits a steeper linear shift. Figure 5b displays the transmission powers for each resonance mode. Interestingly, the transmission power is not linearly related to the slot length, and its values exhibit irregular changes.

3.4. Effect of the width of the intermediate slot (SiO_2)

In the next step, the effect of the slot width of the SiO_2 slot is investigated. The width of this slot is changed from $a = 30$ nm to $a = 150$ nm, and the transmission spectrum is drawn for them. The values of the other parameters are $w = \Delta x = 50$ nm, $L = 500$ nm, $d = 600$ nm, $x = L/2$, and $g = 10$ nm.

Figure 6 shows that two resonance modes can be occurred. The first resonance mode is located in the initial region of the wavelength range, and the second resonance

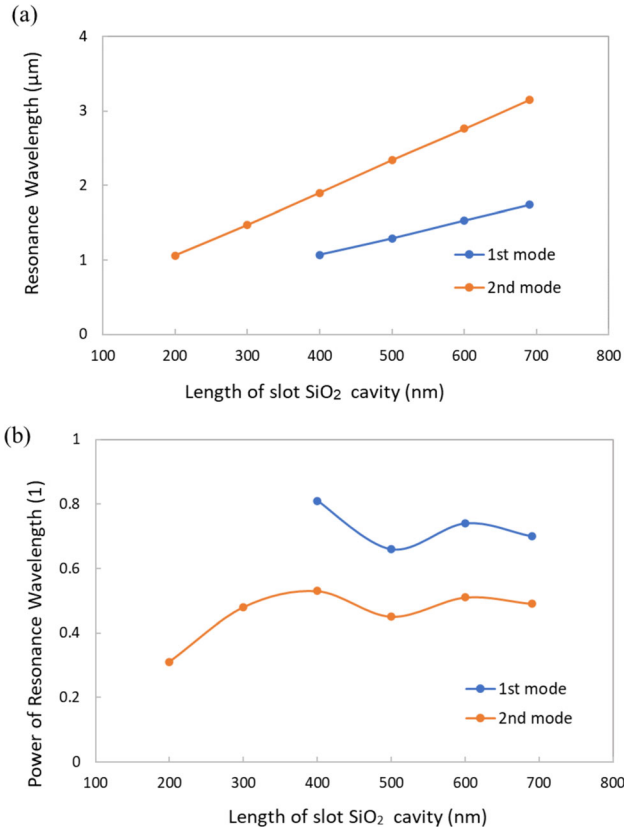


Fig. 5 (a) The first and second resonance wavelengths as a function of the d size. (b) The transmission power of the 1st and 2nd resonance modes as a function of the d size

mode extends to the longer wavelengths. In Fig. 7a, both resonance modes shift to the shorter wavelengths when the width of the silica slot is increased. These results are corresponded to Eqs. (3) and (4). The appeared shift is much greater for the second resonance mode. The transmission power increases with the widening of the slot in the first resonance mode, while it decreases in the second resonance mode.

Figure 7b shows that the transmission power for the first mode increases with the increase in the slot width of the SiO₂ layer. Specifically, at the wavelength of $\lambda = 1.80 \mu\text{m}$ and the slot width $a = 30 \text{ nm}$, the transmission power is about 0.59. As the slot width reaches to $a = 150 \text{ nm}$, the transmission power at the wavelength of $\lambda = 1.16 \mu\text{m}$ increases to 0.88. On the other hand, the transmission power for the second mode decreases as the SiO₂ slot width increases. For instance, at the wavelength of $\lambda = 3.24 \mu\text{m}$ and a slot width of $a = 30 \text{ nm}$, the transmission power is 0.52. However, at the slot width of $a = 150 \text{ nm}$ and the wavelength of $\lambda = 2.21 \mu\text{m}$, the transmission power decreases to 0.38. In addition, the width of the transmission peak decreases with the increases of the slot width.

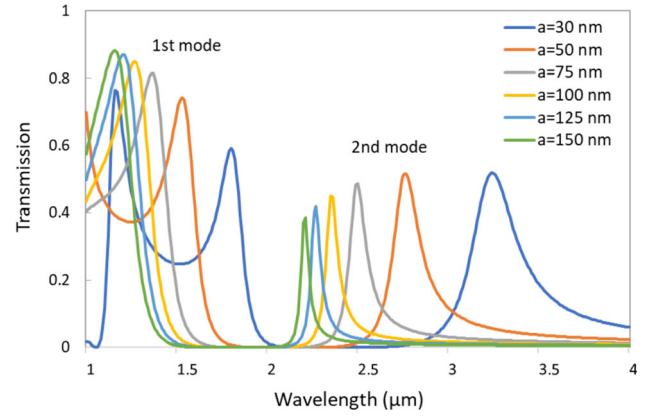


Fig. 6 Transmission spectrum of the proposed filter for different SiO₂ slot widths (a)

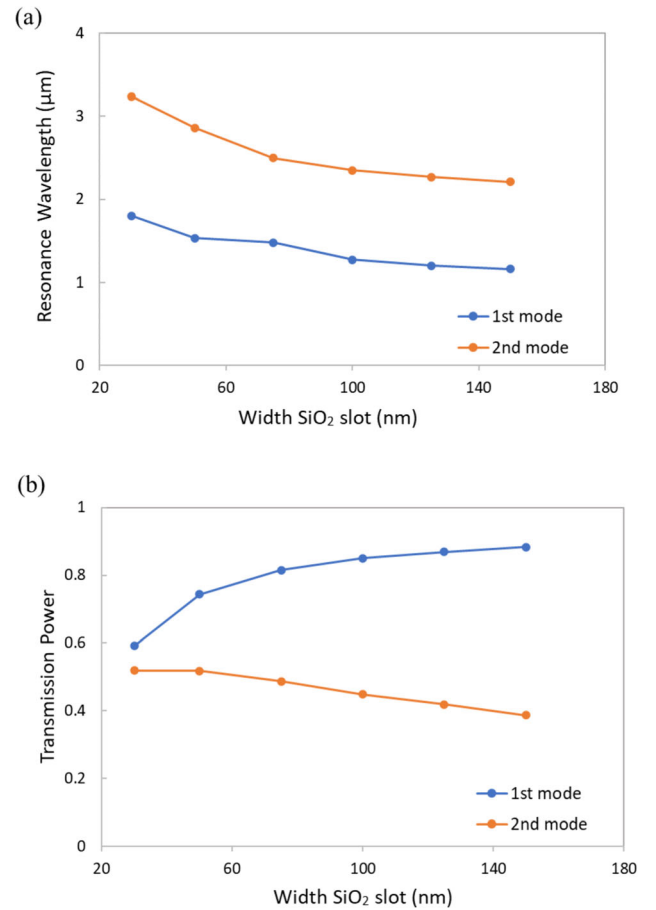


Fig. 7 (a) The 1st and 2nd resonance wavelengths as a function of the a size. (b) The transmission power of the 1st and 2nd resonance modes as a function of the a size

3.5. Effect of the number of intermediate slots (SiO₂)

In the fifth example, the effect of the number of SiO₂ slots is investigated (see Fig. 8). The parameters used in this

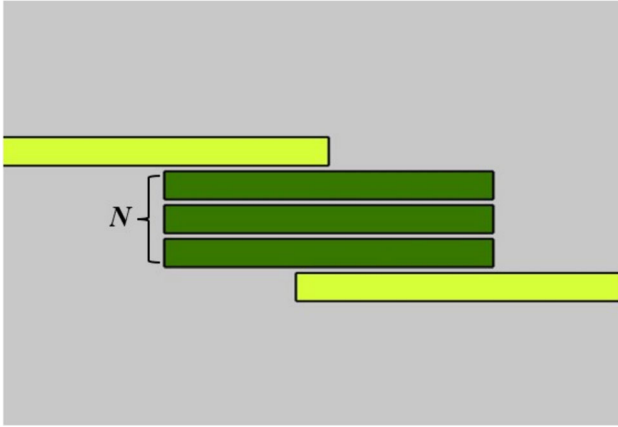


Fig. 8 The MIM plasmonic filter for different numbers of SiO_2 slots (N)

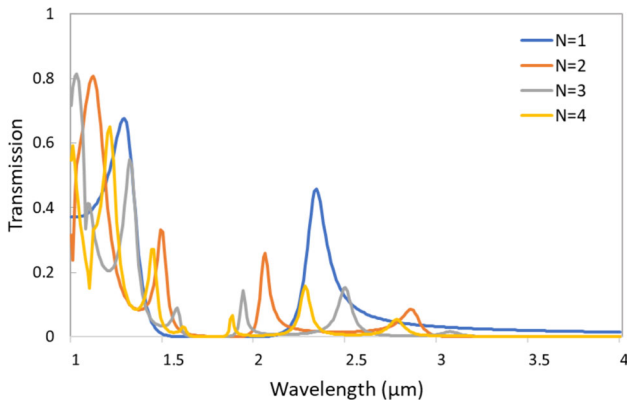


Fig. 9 The transmission spectrum for the MIM plasmonic filter with different numbers of SiO_2 slots when $a = 50$ nm and $d = 500$ nm

structure are as follows: $a = w = \Delta x = 50$ nm, $L = 500$ nm, $d = 500$ nm, $x = L/2$, $g = 10$ nm. By adding the number of slots from one slot to four slots, the number of resonance modes increases. However, only the first resonance modes within the wavelength range of $1 \mu\text{m} - 1.3 \mu\text{m}$ exhibit suitable transmission power. Other resonance modes, have powers less than 0.3. Notably, in the case of $N = 1$, the transmission power for the second mode is approximately 0.5 (see Fig. 9). To create a multi-channel filter, one can add SiO_2 slots. Unfortunately, this approach significantly reduces power, rendering almost no part of the filter practically.

From the simulation of the previous sections, it becomes evident that narrower SiO_2 slot result to the higher transmission power, occurring at the longer wavelengths. Additionally, when the length of the SiO_2 slot equals to $d = 600$ nm, better transmission occurs. Therefore, this simulation is repeated with the SiO_2 slot width of $a = 30$ nm and length $d = 600$ nm, aiming for potentially

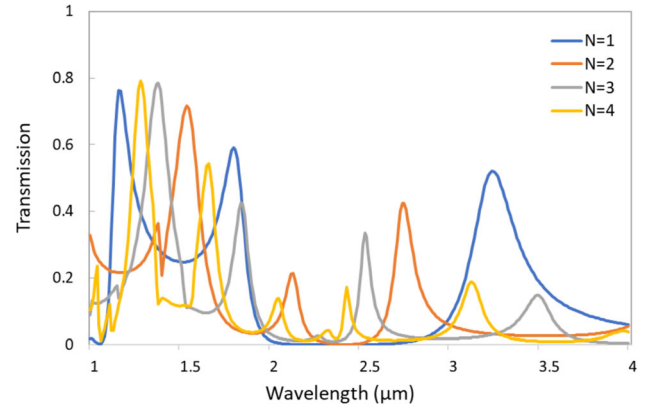


Fig. 10 The transmission spectrum for the MIM plasmonic filter with different numbers of SiO_2 slots when $a = 30$ nm and $d = 600$ nm

improved results. The outcome of this change is satisfactory. The transmission spectrum diagram for the new sample (Fig. 10) reveals that the transmission power of the second mode's peak surpasses the previous state. Although the highest power occurs at $N = 1$, it is not a narrow peak. Interestingly, while the width of the passing peaks in the first mode remains relatively stable with varying the slot numbers, the second mode exhibits a narrower peak when the number of slots increases.

3.6. Two output ports

The ultimate goal is to build a multi-channel plasmonic filter. To achieve this, a sample is designed with two different sizes of the SiO_2 slot: one with a length of $d_1 = 600$ nm and another with a length of $d_2 = 400$ nm. The sample features one input port and one output port (see Fig. 11a). The other filter parameters are $a = w = \Delta x = 50$ nm, $L = 500$ nm, $x = L/2$, and $g = 10$ nm.

Figure 12 displays the transmission spectrum resulting from the simulation of the first sample. Additionally, this figure illustrates the transmission spectrum for the slots with lengths $d = 400$ nm and $d = 600$ nm, facilitating a comparison with double slots. The peaks of the second mode occur at the wavelengths of $\lambda = 1.90 \mu\text{m}$ and $\lambda = 2.77 \mu\text{m}$, for the slot lengths of $d = 400$ nm, and $d = 600$ nm, respectively. At this time, the wave should have passed through two slits as filters, but both stopped. Wavelength $\lambda = 1.53 \mu\text{m}$, associated with the length $d = 600$ nm, undergoes the same filtering process. Hence, apart from the first mode, the others are mostly blocked. However, in the initial range at the wavelength of $\lambda = 1.08 \mu\text{m}$, where both slots permit wave to pass, the SiO_2 double-slot filter allows the transmission. Due to the unfavorable results, we slight adjustments were made to the structure. In the last sample, the SiO_2 slots of the same length as the previous sample were positioned on the both

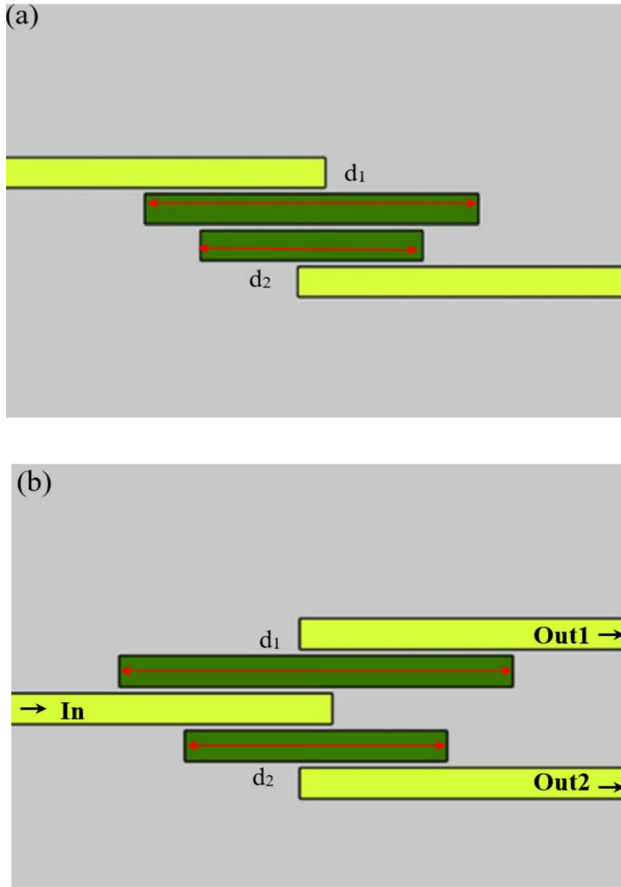


Fig. 11 (a) The MIM plasmonic filter for two different lengths of SiO_2 slots. (b) The MIM plasmonic filter for two output ports

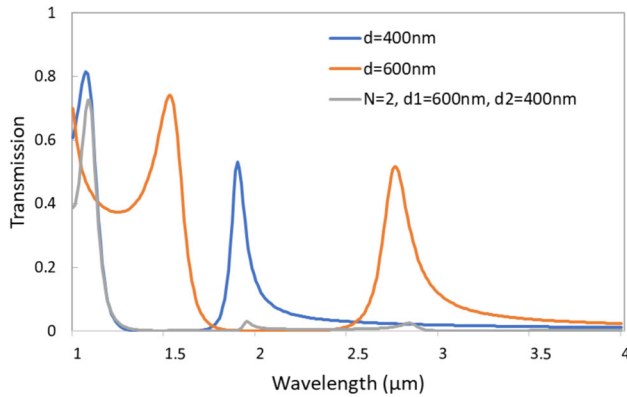


Fig. 12 The transmission spectrum of the proposed filter with a single-slit SiO_2 for lengths of $d = 400$ nm, and $d = 600$ nm, and a filter with two slits of SiO_2 side by side with the same lengths

sides of the air inlet slot, creating two outlet ports adjacent to them (see Fig. 11b). Notably, the spectrum from the simulation is now more favorable (see Fig. 13).

Figure 12 reveals that each SiO_2 slot with the length of $d = 400$ nm and $d = 600$ nm generates two transmission

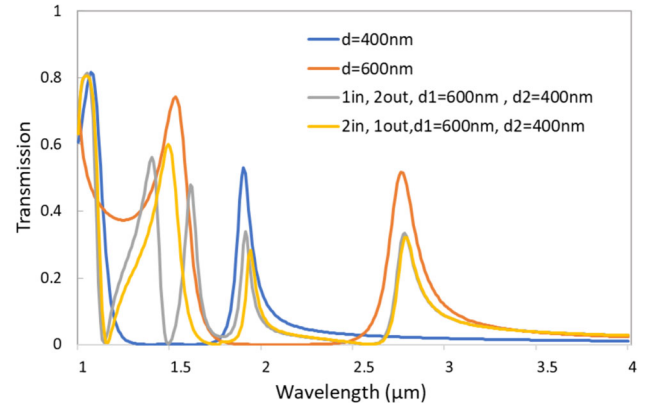


Fig. 13 The transmission spectrum of the proposed filter with a single SiO_2 slit for $d = 400$ nm, a single SiO_2 slit for $d = 600$ nm, two SiO_2 slits for one input port and two output ports (1 in, 2 out), and two SiO_2 slots for two input ports and one Output port (2 in, 1 out)

channels. When combined and utilized concurrently, these yield a 5-channel output spectrum. It seems that except for the first channel, the power of the other channels has decreased (see Fig. 13). For each SiO_2 slot length, there is a separate slot as the output port. The wavelength passing through one slot is not filtered by the other slot, resulting in a final output spectrum with five passing channels. These channels include wavelengths $\lambda = 1.05$ μm , 1.40 μm , 1.61 μm , 1.91 μm , and 2.78 μm , with the transmission powers equal to $P = 0.81, 0.56, 0.48, 0.34,$ and 0.33 , respectively.

If the path is reversed, that means two input ports and one output port are of the previous sizes. The second channels of the single-slot filter with $d = 400$ nm and $d = 600$ nm operate simultaneously, and the two smaller parts in the first channel have been combined into one part with more power. The reason behind this enhancement is the constructive interference of two wavelengths inside the output port (See Fig. 13). The four transmission channels occur at the wavelengths of $\lambda = 1.05$ μm , 1.50 μm , 1.94 μm , and 2.79 μm with the corresponding transmission powers of $P = 0.80, 0.59, 0.28,$ and 0.32 respectively. By implementing these changes, we successfully designed a multi-channel pass filter with an appropriate peak width.

By comparing the results obtained from the simulation of the proposed filter with the previous results [35–39], two advantages of the present study become evident. First, in comparison to the previous structures, the proposed design accommodates the working wavelengths in a broader range, from 1 μm to 4 μm . Second, within this wavelength range, smaller dimensions are suggested for the filter, with narrower width of the passing bandgaps, which is very suitable for filtering. The proposed filter, possessing these properties and based on can find applications in nano-

plasmonic integration circuits, astronomical imaging, and medical diagnostics [38, 39, 41].

4. Conclusion

In this study, an adjustable band-pass plasmonic waveguide filter in the wavelength range of 1–4 μm , consisting of several dielectric slots created inside the metal, is proposed and investigated. The filter structure is based on the Metal/Insulating/Metal (MIM), which included silver metal, air and silica dielectrics. Simulations and investigations confirmed that a tunable multi-channel band-pass filter can be created by controlling the physical and geometrical properties of the proposed waveguide. By placing two slots with different lengths as output channels in this structure, a 5-channel band-pass spectrum can be achieved in the mentioned wavelength range. Thanks to its structure and surface plasmons, this filter has the potential to develop a filter with predictable transmission and band-pass power within the desired ranges. Additionally, the ability to create a multi-channel band-pass filter offers numerous applications, given its compact size and simple design. These applications extend to lithography nanotechnology, nano-scale-integrated circuits, and other areas of nano-electronics research.

References

- [1] J Tao, X Lin, Q Zhang and X Jin *Opt. Express* **17** 13989 (2009)
- [2] N Korani, A Abbasi and M Danaie *Plasmonics* **19** 733 (2024)
- [3] M Danaie, L Hajshahvaladi and E Ghaderpanah *Sci. Rep.* **13** 13976 (2023)
- [4] X Zhang, S Yan, T Li, P Liu, Y Zhang, L Shen, Y Ren and E Hua *Results Phys.* **31** 104997 (2021)
- [5] S M Ebadi, S H Khani and J Örtengren *Opt. Quantum Electron.* **56** 1 (2024)
- [6] Y Qi, P Zhou, T Zhang, X Zhang, Y Wanga, C Liu, Y Bai and X Wang *Results Phys.* **14** 102506 (2019)
- [7] H Zhang, W Zhao, Y Liu, J Chen, X Wang and C Lu *Chinese Phys. B* **30** 117801 (2021)
- [8] V G Achanta *Rev. Phys.* **5** 100041 (2020)
- [9] M Alagdar, B Yousif, N F F Areed and M Elzalabani *Appl. Phys. A* **126** 1 (2020)
- [10] S Khani, M Danaie and P Rezaei *Photonics Nanostructures-Fundam. Appl.* **40** 100802 (2020)
- [11] M R Jafari and F Ebrahimi *J. Sci. Islamic Repub. Iran* **21** 279 (2010)
- [12] M Farhadi, M Jafari and M Shahmansouri *Appl. Phys. A* **126** 1 (2020)
- [13] M R Jafari, F Ebrahimi and M Nooshirvani *J. Appl. Phys.* **108** 054313 (2010)
- [14] S Khani, M Danaie and P Rezaei *J. Comput. Electron* **20** 442 (2021)
- [15] S Paul and M Ray *Plasmonics* **14** 1113 (2019)
- [16] S Khani and M Hayati *Superlattices Microstruct.* **156** 106970 (2021)
- [17] Z Li, Y Wang, T Li, C Huang and Y Zhang *J. Opt.* **50** 495 (2021)
- [18] Y Jia, C Song, Y Liao and H Cai *Electronics* **11** 1370 (2022)
- [19] R F Oulton, V J Sorger, D A Genov, D F P Pile and X Zhang *Nat. Photonics* **2** 496 (2008)
- [20] M Shahmansouri, B Farokhi and R Aboltaman *Phys. Plasmas* **24** 054505 (2017)
- [21] R Aboltaman and M Shahmansouri *Commun. Theor. Phys.* **72** 045501 (2020)
- [22] A Asadi, M R Jafari and M Shahmansouri *Plasmonics* **17** 1819 (2022)
- [23] D Teng, Y Wang, T Xu, H Wang, Q Shao and Y Tang *Nanomaterials* **11** 1281 (2021)
- [24] M Shahmansouri and M Mahmodi-Moghadam *Phys. Plasmas* **24** 102107 (2017)
- [25] M Mahmodi-Moghadam and M Shahmansouri *Physica Scr.* **95** 085606 (2020)
- [26] J Chen, X Wang, F Tang, X Ye, L Yang and Y Zhang *Results Phys.* **16** 102867 (2020)
- [27] A M Heikal, M F O Hameed and S S A Obayya, *Comput. Photonic Sens.* **53** (2019)
- [28] J K Nayak, P R Chaudhuri and P K Sahoo *Appl. Opt.* **60** 7603 (2021)
- [29] T Xu, Y K Wu, X Luo and L J Guo *Nat. Commun.* **1** 1 59 (2010)
- [30] A Said, K S R Atia and S S A Obayya *JOSA B* **37** 11 163 (2020)
- [31] S Elbially, B Yousif and A Samra *Opt. Quantum Electron.* **49** 1 (2017)
- [32] J Jung *Opt. Eng.* **62** 055101 (2023)
- [33] G Challa Ram, P Sambaiah, S Yuvaraj and M V Kartikeyan *AEU Int. J. Electron. Commun.* **170** 154774 (2023)
- [34] I Zegaar, A Hocini, A Harhouz, D Khedrouche and H B Salah *Prog. Electromagn. Res. Lett.* **104** 67 (2022)
- [35] Q Liu, J J Wei, K Gong, H Qian, B H Ma and D W Zhang *IEEE Trans. Circuits Syst. II* **70** 4369 (2023)
- [36] P C Srivastava, L Sharma, K Srivastava and P K Malik *Lecture Notes Electrical Eng.* **2** 13 (2022)
- [37] F Hu and Z Zhou *JOSA B* **28** 10 2518 (2011)
- [38] M R Pav, S P Hosseini, N Granpayeh and A Rahimzadegan *J. Nanophotonic* **12** 1 016010 (2018)
- [39] M J Rieke et al *PASP* **135** 028001 (2023)
- [40] J Tao, X G Huang, X Lin, J Chen, Q Zhang and X Jin *JOSA B* **27** 2 323 (2010)
- [41] Y Liu, H Yuan, F R Kersey, J K Register, M C Parrott and T Vo-Dinh *Sensors* **15** 3706 (2015)

Publisher's Note Springer Nature remains neutral with regard to jurisdictional claims in published maps and institutional affiliations.

Springer Nature or its licensor (e.g. a society or other partner) holds exclusive rights to this article under a publishing agreement with the author(s) or other rightsholder(s); author self-archiving of the accepted manuscript version of this article is solely governed by the terms of such publishing agreement and applicable law.